



Title	Dynamic and nonlinear magnetoconductance: Numerical analysis in two dimensions
Author(s)	Sheng, WD; Zheng, Q; Wang, J; Guo, H
Citation	Physical Review B (Condensed Matter and Materials Physics), 1999, v. 59 n. 1, p. 538-545
Issued Date	1999
URL	http://hdl.handle.net/10722/43286
Rights	Creative Commons: Attribution 3.0 Hong Kong License

Dynamic and nonlinear magnetoconductance: Numerical analysis in two dimensions

Weidong Sheng,* Qingrong Zheng, and Jian Wang

Department of Physics, The University of Hong Kong, Pokfulam Road, Hong Kong, China

Hong Guo

Center for the Physics of Materials and Department of Physics, McGill University, Montreal, PQ, Canada H3A 2T8

(Received 28 July 1998)

We report theoretical investigations on the magnetoconductance of a two-probe two-dimensional mesoscopic conductor in the dynamic and weakly nonlinear transport regimes. Crucial to the investigation is the development of a viable numerical scheme for evaluating functional derivatives of a scattering matrix with respect to the scattering potential landscape in the presence of a magnetic field. The physical behavior of the local partial density of states, the sensitivity, the dynamic conductance, and the second order nonlinear dc conductance as functions of an external uniform magnetic field is revealed at two dimensions. Due to symmetry breaking the magnetic field adds very important effects to these physical quantities.

[S0163-1829(99)07401-9]

I. INTRODUCTION

Quantum transport properties of mesoscopic conductors under the influence of an external magnetic field \mathbf{B} have been intensively investigated for a variety of reasons, both theoretically and experimentally. The theoretical studies have so far concentrated on the behavior of linear dc magnetoconductance as motivated by the quantum Hall effects¹ and universal conductance fluctuation phenomenon.² In this paper we will move forward to investigate the magnetoconductance in linear ac and nonlinear dc transport regimes of a two dimensional (2D) mesoscopic conductor. The ac and nonlinear dc transport involve new physics,³⁻¹¹ namely, dynamic induction and gauge invariance. They are very important for practical applications as many electronic devices operate under ac and nonlinear conditions. When there is an external magnetic field, some important symmetry properties of conductance may be broken^{3,12} and it is interesting to investigate these symmetry properties. ac and nonlinear dc transport properties depend on several physical quantities which do not play a role in the familiar linear dc situations: the various local partial density of states (LPDOS),¹³ the sensitivity,¹⁴ the functional derivatives of the scattering matrix, and quantities related to them. These physical quantities depend on magnetic field in an essential way and we reveal this relationship.

It has now been well established that the quantum transport formalism which maintains electric current conservation under ac fields must include effects of the internal potential response of a conductor.³ This internal potential response comes due to electron-electron interactions and it generates such effect as a displacement current. In addition to the conservation law, a correct theory must also guarantee gauge invariance: the outcome of a theory should not change when potential everywhere is raised by the same constant amount. The gauge invariance must be carefully taken into account when dealing with *nonlinear* effects where powers of voltages appear in a theory. It has been confirmed that the internal potential plays the essential role in providing gauge in-

variance at the nonlinear order.³ Hence it is crucial for practical calculations to evaluate the contribution of internal potential to the dynamic and nonlinear conductance.

Within the scattering matrix formalism,³ the internal potential response of the conductor alters the scattering matrix $\mathbf{s}_{\alpha\beta}$ in essential ways. Let us consider the dynamic conductance $G_{\alpha\beta}(\omega)$ to first order in ac frequency ω , as given by³ $G_{\alpha\beta}(\omega) = G_{\alpha\beta}(0) - i\omega e^2 E_{\alpha\beta} + O(\omega^2)$, where $G_{\alpha\beta}(0)$ is the linear dc conductance and $E_{\alpha\beta}$ is the emittance. $E_{\alpha\beta}$ has two terms:³ an external contribution given by the global partial density of states (GPDOS) and an internal contribution determined by the local partial density of states (LPDOS). While the GPDOS can be calculated straightforwardly using numerical derivatives,¹⁵ the LPDOS is given by quantities such as $\delta\mathbf{s}_{\alpha\beta}/\delta U(\mathbf{r})$, where the functional derivative of the scattering matrix $\mathbf{s}_{\alpha\beta}$ is taken with respect to the internal potential landscape $U(\mathbf{r})$. Clearly, this functional derivative is extremely difficult to evaluate for mesoscopic conductors with complicated scattering boundaries. This is the reason that so far the only known results about these quantities are for a few very simple cases^{14,16} even without a magnetic field. Hence quantum transport in mesoscopic systems under ac and nonlinear dc conditions have not been investigated extensively although the theoretical formalism has been well established.³ In addition, it has been demonstrated that LPDOS also plays an important role in the physics associated with weakly nonlinear dc conductance coefficient.¹⁷ There, the above functional derivative enters through the so-called sensitivity¹⁴ which measures the local electric current response. So far only two reports have appeared in the literature^{16,18} concerning nonlinear conductances which dealt with systems without a magnetic field. Finally, there are interesting magnetic field dependences of the functional derivative which leads to the interesting symmetry properties of the LPDOS.¹⁹

Without a magnetic field, there is now a way to numerically compute¹⁸ the functional derivative $\delta\mathbf{s}(E)_{\alpha\beta}/\delta U(\mathbf{r})$. The first part of this paper reports the necessary extensions of the method of Ref. 18 to include a magnetic field. In the

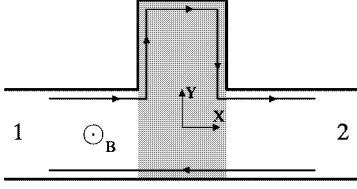


FIG. 1. Schematic view of a T-shaped quantum wire. The wire width, the side-stub width and height is W . The shaded area stands for the scattering region.

main section we report the magneto conductance properties of a 2D conductor, shown in Fig. 1, in the ac and second order weakly nonlinear dc regimes. This conductor behaves as a quantum interference transistor²⁰ and has been the subject of extensive studies in the linear dc situations. We pay special attention to the symmetry breaking properties of the magnetic field on various physical quantities.

Before presenting the details of the calculation, we summarize the main results of this work. (1) A general and widely applicable numerical scheme is developed for ac and nonlinear dc transport within a finite magnetic field. (2) An interesting spatial symmetry is found for conductors which possesses the property that its potential is symmetrical along the transport direction. (3) The establishment of edge channels due to magnetic field suppresses transport resonances and leads to a largely inductive ac response. (4) The electric current response as measured by sensitivity shows another interesting spatial symmetry for geometrically symmetrical conductors along the transport direction. (5) A finite magnetic field leads to a finite second order nonlinear dc conductance for a geometrically symmetrical conductor which would be zero without the field. (6) By tuning the strength of the magnetic field, a large and negative second order nonlinear conductance result: this has important implications to the nonlinear I - V curves.

II. NUMERICAL METHOD

Throughout the discussion, we shall assume quantum coherence within the 2D conductor. To find the scattering matrix in a magnetic field, there are several known methods such as mode-matching,²¹ finite-element,²² and recursive Green's function.²⁰ However, these methods are not particularly suitable for calculating the functional derivative $\delta S_{\alpha\beta}/\delta U(\mathbf{r})$. For this purpose, we found that a numerical technique developed for computing scattering matrix in the absence of magnetic field, reported in Ref. 23, to be quite useful.

To make the discussion of our method more specific, without losing generality, we use the T-shaped 2D conductor in Fig. 1 as the example. We divide it into three uniform sections: two for the straight probes and one for the scattering region (the side-arm region). For more complicated shapes with two probes we divide it into enough sections such that the potential inside each section can be safely assumed to be independent of the coordinate along the transport direction. For each section the corresponding scattering matrix is computed by the mode-matching method. Finally, a global scattering matrix is constructed by a composition of all the individual scattering matrices

$$\mathbf{S} = \mathbf{S}_1 \otimes \mathbf{S}_2 \otimes \cdots \otimes \mathbf{S}_{M-1}, \quad (1)$$

where \mathbf{S}_n is the scattering matrix associated with the n th section, \otimes is the operator and stands for the composition of two scattering matrices,²⁴ and M is the total number of sections.

The scattering matrix \mathbf{S}_n describes two scattering processes associated with the n th section, free propagation from the left end to its right end and interface scattering due to the potential discontinuity at the interface between the n th and $(n+1)$ th section. Therefore it can be expressed as the composition of two individual scattering matrices

$$\mathbf{S}_n = \mathbf{S}_n^f \otimes \mathbf{S}_n^i. \quad (2)$$

Here \mathbf{S}_n^f describes the free propagation and is given by

$$\mathbf{S}_n^f(L_n) = \begin{bmatrix} \mathbf{0} & \mathbf{P}_n^- \\ \mathbf{P}_n^+ & \mathbf{0} \end{bmatrix}, \quad (3)$$

where $\mathbf{P}_n^\pm = \exp(\pm i\mathbf{K}_n^\pm L_n)$, \mathbf{K}_n^+ (\mathbf{K}_n^-) is a diagonal matrix whose diagonal elements are the wave numbers of the right(left)-going transverse modes, and L_n is the length of the n th section. \mathbf{S}_n^i describes the interface scattering and can be solved using the mode-matching technique.²³

In the presence of a perpendicular uniform magnetic field B , it is convenient to choose the vector potential as $\mathbf{A} = (-By, 0, 0)$. For the n th section, the longitudinal wave number and transverse wave function satisfy

$$\left[-\frac{\hbar^2}{2m^*} \frac{d^2}{dy^2} + \frac{m^* \omega_c^2}{2} (y - l_B^2 k_{n,m})^2 + V_n(y) \right] \phi_{n,m}(y) = E_F \phi_{n,m}(y), \quad (4)$$

where $\omega_c = eB/m^*$ is the cyclotron frequency, $l_B = \sqrt{\hbar/eB}$ is the magnetic length, and E_F the Fermi energy. According to the group velocity which is given by

$$v_{n,m} = \hbar/m^* \langle \phi_{n,m} | k_{n,m} - y/l_B^2 | \phi_{n,m} \rangle, \quad (5)$$

the transverse states can be classified into two categories: the right-going states $\phi_{n,m}^+$ with purely positive real or positive imaginary $v_{n,m}$ and left-going states $\phi_{n,m}^-$ with purely negative real or negative imaginary $v_{n,m}$. In our numerical calculations, we expand the transverse wave functions $\phi_{n,m}^\pm(y)$ in terms of those of $B=0$ denoted by $\varphi_{n,j}(y)$,

$$\phi_{n,m}^\pm(y) = \sum_j (F_n^\pm)_{jm} \varphi_{n,j}(y). \quad (6)$$

The coefficients $(F_n^\pm)_{jm}$ form the matrices \mathbf{F}_n^\pm . The number of terms necessary for numerical convergence depends on the strength of B . We shall use a dimensionless quantity $\beta = \hbar\omega_c/E_1$ to denote the strength where E_1 is the threshold of the first transverse energy subband in the absence of B . For $\beta=1.0$, the number of terms in the expansion (6) should be at least 30. Finally, the coupling between the transverse

states when $B=0$ in the two adjacent sections is denoted by the coupling coefficients $C_{ij} \equiv \langle \varphi_{n,i} | \varphi_{n+1,j} \rangle$ which construct matrix \mathbf{C} .

The *global scattering matrix* \mathbf{S} calculated this way, which connects all outgoing waves to incoming waves, included the decaying modes. Thus \mathbf{S} does not satisfy the unitary condition. \mathbf{S} is different from the physical scattering matrix²⁵ which only connects propagating waves. In order to obtain the physical scattering matrix which we denote by the lower case \mathbf{s} , we first rewrite global \mathbf{S} in the form of 2×2 sub-blocks and obtain four submatrices \mathbf{S}_{ij} where $(i,j=1,2)$. Then for each submatrix \mathbf{S}_{ij} , we build a new matrix \mathbf{s}_{ij} constructed by the first N_0 rows and columns of \mathbf{S}_{ij} , where N_0 is the number of propagating channels. By writing the four newly constructed matrices in the form of 2×2 blocks, a $2N_0$ -dimensional scattering matrix \mathbf{s} is obtained which is the true scattering matrix. In order to obtain a unitary scattering matrix \mathbf{s} , one should further take a unitary transformation:

$$\mathbf{s} = \mathbf{A} \mathbf{s} \mathbf{A}^{-1},$$

$$\mathbf{A} = \begin{bmatrix} \mathbf{V}_1 & \mathbf{0} \\ \mathbf{0} & \mathbf{V}_M \end{bmatrix}, \quad (7)$$

where \mathbf{V}_1 and \mathbf{V}_M is N_0 -dimensional diagonal matrices with respective diagonal element $\sqrt{v_{1,m}^+}$ and $\sqrt{v_{M,m}^+}$.

To compute $\delta \mathbf{s}_{\alpha\beta} / \delta U(\mathbf{r})$, we shall add a δ -function scatterer inside the scattering region with an infinitesimal scattering strength γ , $V(\mathbf{r}) = \gamma \delta(\mathbf{r} - \mathbf{r}_0)$. The position of the impurity $\mathbf{r} = \mathbf{r}_0$ is arbitrary inside the scattering region. We then calculate $\mathbf{s}_{\alpha\beta}$ as a function of γ . Once done, we use a five-point numerical derivative to evaluate $\delta \mathbf{s}_{\alpha\beta} / \delta U(\mathbf{r}) \equiv \partial \mathbf{s}_{\alpha\beta} / \partial \gamma |_{\gamma=0}$ thus obtaining various LPDOS.

The problem of solving scattering matrix in the presence of the extra scatterer is more complicated, but it can still be done using the above approach.²⁴ Here we give the useful expressions. Suppose the δ -function scatterer is located in the n th section at position $\mathbf{r}_0 = (x_0, y_0)$, where (x_0, y_0) is the distance from the left and from the bottom boundary of that section. The scattering matrix associated with this section is then given by

$$\mathbf{S}_n = \mathbf{S}_n^f(x_0) \otimes \mathbf{S}_n^\delta \otimes \mathbf{S}_n^f(L_n - x_0) \otimes \mathbf{S}_n^i, \quad (8)$$

where \mathbf{S}_n^δ describes the scattering process associated with the δ -function scatterer and is given by

$$\mathbf{S}_n^\delta = \begin{bmatrix} -\mathbf{F}_n^- & \mathbf{F}_n^+ \\ -\mathbf{\Gamma} \mathbf{F}_n^- - i \mathbf{F}_n^- \mathbf{K}_n^- & i \mathbf{F}_n^+ \mathbf{K}_n^+ \end{bmatrix}^{-1} \times \begin{bmatrix} \mathbf{F}_n^+ & -\mathbf{F}_n^- \\ \mathbf{\Gamma} \mathbf{F}_n^+ + i \mathbf{F}_n^+ \mathbf{K}_n^+ & -i \mathbf{F}_n^- \mathbf{K}_n^- \end{bmatrix}, \quad (9)$$

where the matrix $\mathbf{\Gamma}$ describes the mode-mixing effect due to the δ -function scatterer and its matrix elements are given by $\Gamma_{pq} = 2\gamma \sin(p\pi y_0/W_n) \sin(q\pi y_0/W_n)/W_n$. With the δ function included this way, one can again apply Eq. (1) to

compute the scattering matrix $\mathbf{s} = \mathbf{s}(\gamma)$ and complete the numerical derivatives discussed in the last paragraph.

To end this section, we discuss two important points in the computation of scattering matrix. The first concerns the normalization of transverse wave functions. In addition to the conventional normalization condition

$$\sum_i |(F_n^\pm)_{ij}|^2 = 1, \quad (10)$$

the expansion coefficients should satisfy another condition, i.e., for each n and j , $(F_n^\pm)_{ij}$ with the maximum norm should be purely real. This condition is naturally satisfied in the case of $B=0$. The second point is the order of the wave numbers in \mathbf{K}_n^\pm . In the numerical calculations, we find that the order of the wave numbers in \mathbf{K}_n^+ should be the same as those in \mathbf{K}_n^- , i.e., $v_{n,m}^+ = -v_{n,m}^-$. If neither of the two conditions is satisfied, the numerically calculated scattering matrix would not be unitary.

III. RESULTS

Using the numerical technique developed in the last section, we now investigate magneto conductance of the 2D conductor shown in Fig. 1. This system has been studied before^{20,15,18} in the absence of a magnetic field. The effects of a finite magnetic field B is to push the electron sideways and that breaks the symmetry of LPDOS which has important consequences to the ac and nonlinear conductances (see below). In all the results to be presented below, the direction of the magnetic field \mathbf{B} is pointing out of the page of Fig. 1.

A. Local density of states

For dynamic conductance $G_{\alpha\beta}(\omega)$ up to the linear order of ac bias frequency ω , and for second order weakly nonlinear dc conductance $G_{\alpha\beta\gamma}$, the relevant LPDOS are the emissivity $dn(\alpha, \mathbf{r})/dE$ and injectivity $dn(\mathbf{r}, \alpha)/dE$. Here the emissivity is defined as³

$$\frac{dn(\alpha, \mathbf{r})}{dE} = -\frac{1}{4\pi i} \sum_\beta \text{Tr} \left(\mathbf{s}_{\alpha\beta}^\dagger \frac{\delta \mathbf{s}_{\alpha\beta}}{\delta e U(\mathbf{r})} - \mathbf{s}_{\alpha\beta} \frac{\delta \mathbf{s}_{\alpha\beta}^\dagger}{\delta e U(\mathbf{r})} \right) \quad (11)$$

and the injectivity is given by¹³ the scattering wave functions

$$\frac{dn(\mathbf{r}, \gamma)}{dE} = \sum_n \frac{|\Psi_{\gamma n}(\mathbf{r})|^2}{h v_{\gamma n}}, \quad (12)$$

where $v_{\gamma n}$ is the electron velocity for the propagating channel labeled by n . The physical meaning of these quantities has been carefully discussed in the literature:¹⁴ emissivity describes the DOS for exiting the conductor from a particular probe while injectivity gives the DOS of injecting into the conductor from a particular probe. When $B=0$, these two are identical to each other¹⁴ at any space point \mathbf{r} . When $B \neq 0$ they do not equal, although from the general microreversibility property of the scattering matrix, it can be shown that³

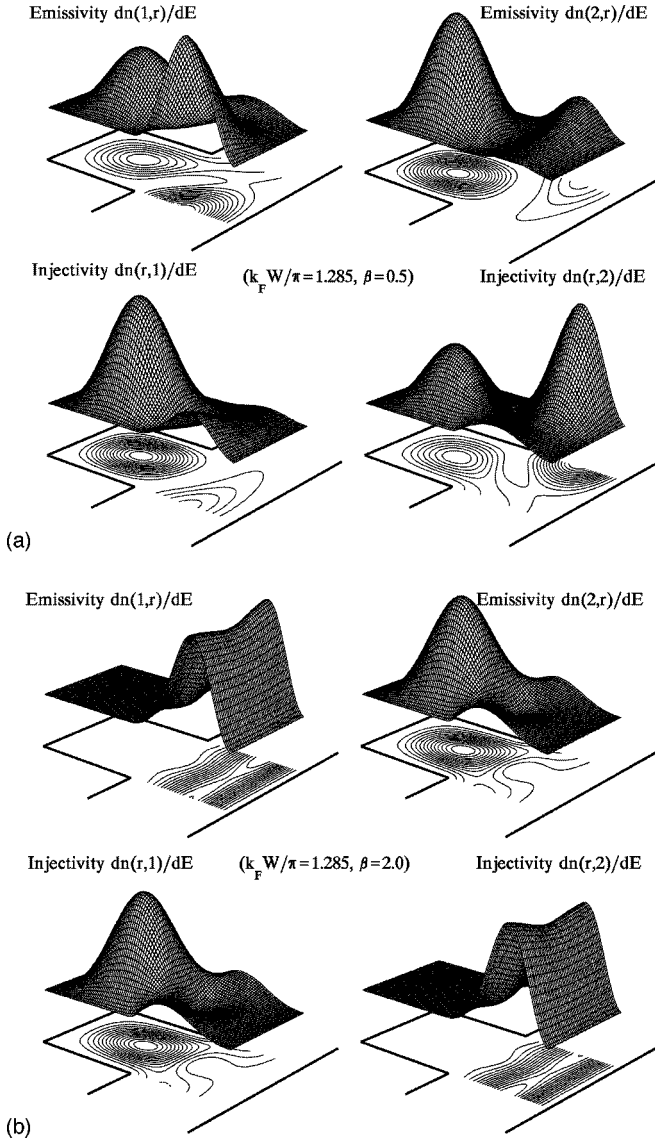


FIG. 2. Three-dimensional view of the emissivity $dn(\alpha, \mathbf{r})/dE$ and injectivity $dn(\mathbf{r}, \alpha)/dE$ at $k_F W/\pi = 1.285$. (a) $\beta = 0.5$, (b) $\beta = 2.0$.

$$\frac{dn(\alpha, \mathbf{r}, \mathbf{B})}{dE} = \frac{dn(\mathbf{r}, \alpha, -\mathbf{B})}{dE}. \quad (13)$$

Figure 2 shows these LPDOS for $B \neq 0$ in the entire scattering region (the shaded area of Fig. 1) where we used magnetic field parameter $\beta = 0.5$ and $\beta = 2.0$ (β is defined in Sec. II), the electron energy is given by $k_F W/\pi = 1.285$, where W is the width of the lead. Our numerical results presented in Fig. 2 suggest the following interesting symmetry:

$$dn[1(2), x, y, \mathbf{B}]/dE = dn[-x, y, 2(1), \mathbf{B}]/dE, \quad (14)$$

where x is the transport direction. Thus for this conductor there is a spatial antisymmetry along the transport direction between the two LPDOS. In fact Eq. (14) is a general result whenever the scattering potential is symmetric along the transport direction, because we can then set the origin of the coordinate system such that the potential has a spatial inverse symmetry. A consequence is $dn[1(2), x, y, B]/dE$

$= dn[2(1), -x, y, -B]/dE$ due to this inverse symmetry. Combining this with Eq. (13) we thus derive the general form of Eq. (14).

The spatial dependence of LPDOS is related to the magnetic field strength. When B is not strong [e.g., Fig. 2(a) with $\beta = 0.5$], the edge states have not formed and an usual picture of wave propagation is found. The large LPDOS inside the side-arm region is due to the scattering electron energy which happens to be a resonance reflection point: at resonance the electron dwells a long time inside the scattering volume leading to a large LPDOS there. Due to magnetic field, incoming from lead 1 or from 2 give very different LPDOS as expected: $dn(r, 2)/dE \neq dn(r, 1)/dE$. Very different LPDOS is obtained for a strong magnetic field as demonstrated in Fig. 2(b) with the parameter $\beta = 2.0$. Due to Lorentz force, electrons coming from probe 1 (see Fig. 1) is pushed upward while that from probe 2 downward. Figure 2(b) shows a clear ‘‘edge channel’’ when injecting from probe 2, see $dn(r, 2)/dE$ of the lower-right panel. As the edge channel propagates along the lower boundary of the structure it is hardly scattered by the potential, therefore little LPDOS is found in the side stub of the 2D wire. When incident from probe 1, LPDOS $dn(r, 1)/dE$ shows an edge channel in the right-going direction along the upper boundary, resulting to a large LPDOS in the side stub. These features due to a finite \mathbf{B} leads to corresponding behavior in dynamic as well as nonlinear conductances to be presented next.

B. Dynamic conductance

In the scattering matrix theory³ the dynamic conductance $G_{\alpha\beta}(\omega)$ to first order in ac frequency ω can be determined completely from first principles:

$$G_{\alpha\beta}(\omega) = G_{\alpha\beta}(0) - i\omega e^2 E_{\alpha\beta} + O(\omega^2),$$

where $G_{\alpha\beta}(0)$ is the dc conductance, $E_{\alpha\beta}$ is the emittance,¹³ and α (or β) labels the probe. The emittance $E_{\alpha\beta}$ describes the current response at probe α due to a variation of the electrochemical potential at probe β to leading order with respect to frequency ω . It can be written as^{3,26}

$$E_{\alpha\beta} = \int d\mathbf{r}^3 dn_{\alpha\beta}(\mathbf{r})/dE - \int d\mathbf{r}^3 [dn(\alpha, \mathbf{r})/dE] u_{\beta}(\mathbf{r}),$$

where the $dn_{\alpha\beta}/dE$ is the local partial density of states¹⁴ which is related to the scattering matrix:

$$\frac{dn_{\alpha\beta}}{dE} = -\frac{1}{4\pi i} \left(s_{\alpha\beta}^{\dagger} \frac{ds_{\alpha\beta}}{e\delta U(\mathbf{r})} - \frac{ds_{\alpha\beta}^{\dagger}}{e\delta U(\mathbf{r})} s_{\alpha\beta} \right). \quad (15)$$

Here $u_{\beta}(\mathbf{r})$ is the characteristic potential which measures the variation of the potential landscape of the scattering volume due to the perturbation.³ Within the Thomas-Fermi screening model, it is given by

$$u_{\beta}(\mathbf{r}) = \frac{dn(\mathbf{r}, \beta)/dE}{dE} \bigg/ \frac{dn(\mathbf{r})}{dE}. \quad (16)$$

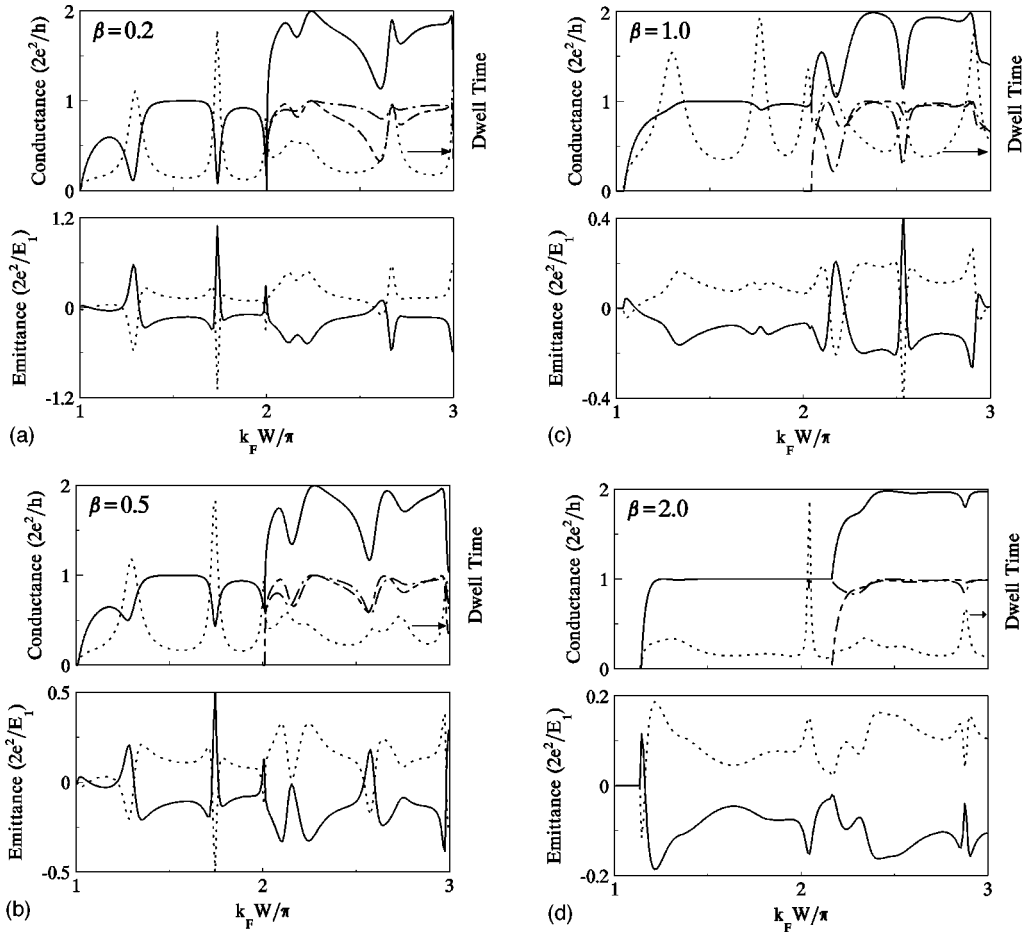


FIG. 3. The dc conductance G_{11} , dwell time τ_1 , partial transmission coefficients T_1 and T_2 , and emittance E_{11} and E_{12} as a function of the normalized electron momentum $k_F W / \pi$. Here $E_1 = (\pi/W)^2 \hbar^2 / (2m)$. In the upper panel, the solid lines stand for G_{11} , dotted lines for τ_1 , solid-dotted lines for T_1 , and solid-dash lines for T_2 . In the lower panel, the solid lines stand for E_{11} and dotted lines stand for E_{12} . (a) $\beta = 0.2$, (b) $\beta = 0.5$, (c) $\beta = 1.0$, (d) $\beta = 2.0$.

Here $dn(\mathbf{r})/dE = \sum_{\beta} dn(\mathbf{r}, \beta)/dE$ is total local partial density of states. Equation (16) is obtained by applying the quasineutrality approximation³ which avoids the solution of the Poisson equation numerically. In this approximation the charge polarization in the system is neglected.

In this section we investigate emittance $E_{\alpha\beta}$ as \mathbf{B} is varied. Because this physical quantity, which is experimentally measurable, has never been obtained within a finite magnetic field for typical 2D conductors, we shall thus present some detailed information of it.

The 2D conductor of Fig. 1 is in general very transmissive from probe 1 to 2, thus the linear dc conductance is usually large (in units of $2e^2/h$) for the whole range of the incident electron energies.^{20,15} The only transport anomalies arise due to resonance reflection at which transmission coefficient equals zero.^{20,15} The resonance behavior comes when the incident electron energy matches that of a scattering state in the scattering region of the conductor. In a previous investigation we have found¹⁵ that when $\mathbf{B} = 0$, $E_{\alpha\beta}$ is also dominated by the same quantum resonances, and inductive as well as capacitive responses can be obtained near a resonance. When $\mathbf{B} \neq 0$, the current response can be drastically different from that of zero field case, depending on the strength of \mathbf{B} . In general for a small \mathbf{B} , e.g., up to $\beta \sim 0.5$, $E_{\alpha\beta}$ is similar to the $\mathbf{B} = 0$ studied before.¹⁵

Because the main effect of a strong \mathbf{B} is to establish edge channels, such a field in general should diminish the quantum resonance in the dc transmission thereby alter the dynamic response. Figure 3 shows, for four field strengths $\beta = 0.2, 0.5, 1.0$, and 2.0 , the dc conductance G_{11} , the dwell time τ_1 , partial transmission coefficients T_1 and T_2 , and emittance E_{11} and E_{12} , as a function of the normalized electron momentum $k_F W / \pi$. Comparing with the $\mathbf{B} = 0$ results,¹⁵ several important differences are observed. First, the edge channel makes dc conductance steplike instead of resonancelike, thus the large peaks in emittance when $\mathbf{B} = 0$ seen previously¹⁵ are suppressed. These peaks (when $\mathbf{B} = 0$) were due to drastic changes of LPDOS at a resonance. Thus edge channels destroy them. Hence for reasonably strong magnetic field, our result predicts a rather smooth emittance profile as a function of scattering electron energy. Second, for large \mathbf{B} , e.g., when parameter $\beta = 2.0$, the entire emittance profile takes negative value (except at the onset of transport when energy is small). Thus the electric current response is entirely inductive which is consistent with the establishment of edge channel. For small or zero \mathbf{B} , both capacitive and inductive responses are possible. Our results thus predict a change of ac response character as the magnetic field strength is increased. This is a reasonable result because a

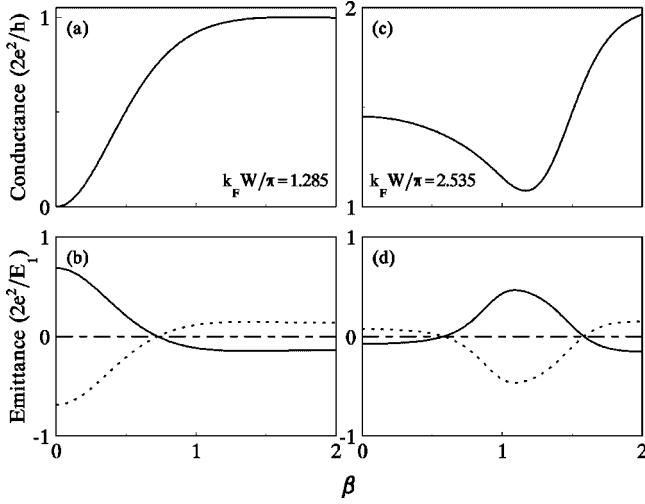


FIG. 4. The emittance E_{11} and E_{12} as a function of the strength of the magnetic field β for two different values of the electron momentum: (a) and (b) $k_F W/\pi=1.285$, (c) and (d) $k_F W/\pi=2.535$. Here $E_1=(\pi/W)^2\hbar^2/(2m)$.

capacitive response tends to be linked with situations which do not conduct dc current, and the edge channels help transmission leading to the inductive response. Third, while the dc conductance is already steplike in strong \mathbf{B} , there are still some fluctuations in the emittance profile [Fig. 3(b)] especially above $k_F W/\pi > 2.0$. This behavior is also related to edge channel formation. For $k_F W/\pi > 2.0$, there exist two propagating modes for this range of \mathbf{B} both contribute to emittance. These modes give transmission coefficients T_1 and T_2 which are plotted in the upper panels of Fig. 3. It is clear that T_1 has a smoother profile than T_2 because T_1 corresponds to the mode which is spatially closer to the conductor edge. The mode with T_2 is further away from the edge, thus is influenced more by the scattering potential. It is the mode with T_2 which gives the fluctuations in the emittance profile. This result suggests an interesting experiment to *directly* investigate the formation of edge channels by measuring the dynamic current response as the magnetic field is increased.

Our magnetoconductance results are summarized in Fig. 4 for two electron Fermi energies. Figure 4(a) is for $k_F W/\pi = 1.285$ which is a resonance point ($T=0$ in the T-shaped structure) when $\mathbf{B}=0$. We observe that both the dc conductance and emittance are monotonic functions of the magnetic field. This is because that only one conducting mode exists. When $\beta > 0.7$, E_{11} changes sign, i.e., the response changes from a capacitive-like conductor to an inductive-like conductor. E_{11} becomes constant for even larger β : once a perfect edge channel is formed, the ac response cannot change anymore. This is consistent with the result of Ref. 4 where for a Corbino disk at $T=0$ (near resonance in our case) the emittance is positive and for a Hall bar the emittance is negative. Figures 4(b) is for $k_F W/\pi = 2.535$, the curves are no longer monotonic of the magnetic field because of the competition between the two conducting modes. Again, a large \mathbf{B} makes the response inductive.

C. Nonlinear dc conductance

Under a weak bias situation, the dc transport may be analyzed order by order in terms of the bias. The scattering

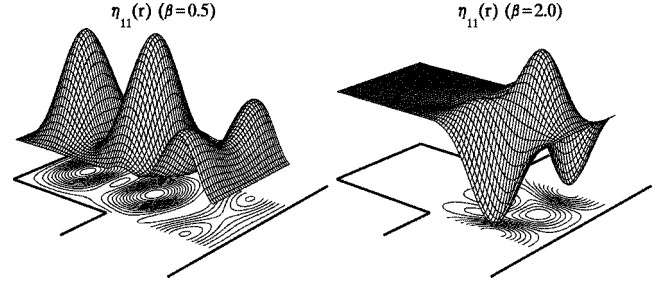


FIG. 5. Three-dimensional view of the sensitivity $\eta_{11}(\mathbf{r})$ at $k_F W/\pi=1.735$. Left panel, $\beta=0.5$ and right panel, $\beta=2.0$.

matrix theory allows the analysis of the second order nonlinear conductance¹⁷ provided that the LPDOS are known. In this section we present results of the second order weak bias nonlinear dc conductance defined by expanding the electric current to second order in bias: $I_\alpha = \sum_\beta G_{\alpha\beta} V_\beta + \sum_{\beta\gamma} G_{\alpha\beta\gamma} V_\beta V_\gamma$, where¹⁷

$$G_{\alpha\beta\gamma} = 4\pi \frac{e}{h} \int dE (-\partial_{Ef}) \int d^3\mathbf{r} [\eta_{\alpha\beta} u_\gamma(\mathbf{r}) + \eta_{\alpha\gamma} u_\beta(\mathbf{r}) - \eta_{\alpha\beta} \delta_{\gamma\beta}] \quad (17)$$

and

$$\eta_{\alpha\beta}(\mathbf{r}) = \frac{1}{4\pi} \frac{\delta A_{\alpha\beta}}{\delta U(\mathbf{r})} = -\frac{1}{4\pi} \text{Tr} \left(\mathbf{s}_{\alpha\beta}^\dagger \frac{\delta \mathbf{s}_{\alpha\beta}}{\delta U(\mathbf{r})} + \mathbf{s}_{\alpha\beta} \frac{\delta \mathbf{s}_{\alpha\beta}^\dagger}{\delta U(\mathbf{r})} \right) \quad (18)$$

is the *sensitivity*¹⁴ which measures the local electric current response to an external perturbation. In Eq. (17), the first two terms are the local contribution G_{111}^i due to the internal potential and the third term corresponds to the external response G_{111}^e . A calculation of general I - V curve has been performed¹⁷ in 1D where approximate scattering matrix can be used for the discussion. For a one-dimensional double barrier tunneling structure $G_{\alpha\beta\gamma}$ has been calculated exactly.²⁷ In the absence of magnetic field, $G_{\alpha\beta\gamma}$ has been obtained for the T-shaped structure¹⁸ and a special 2D conductor through the exact solution.¹⁶ Our numerical technique presented here allows a general analysis within a finite \mathbf{B} .

The nonlinear dc conductance depends on LPDOS as well as sensitivity which is calculable from the functional derivatives $\delta \mathbf{s}_{\alpha\beta} / \delta U(\mathbf{r})$. The sensitivity $\eta_{\alpha\beta}$ is an important physical quantity although it is perhaps difficult to measure experimentally. Figure 5 plots this quantity in the scattering region of the conductor for two values of magnetic field. For $\beta=0.5$ and $k_F W/\pi=1.735$, which is on resonance, η_{11} behaves as a standing wave which is in accordance to the usual quantum resonance picture. Thus the electric current response is generally large inside the entire scattering region. For $\beta=2.0$ where edge states form, the sensitivity shows oscillations only in the quantum wire region where an edge state traverses, the current response is small inside the side-stub. Our numerical results also confirms the relationship $\eta_{12} = \eta_{21} = -\eta_{11} = -\eta_{22}$ at any space point \mathbf{r} . This relationship is a consequence of the unitary condition for scattering matrices.¹⁴ For the particular 2D conductor studied here,

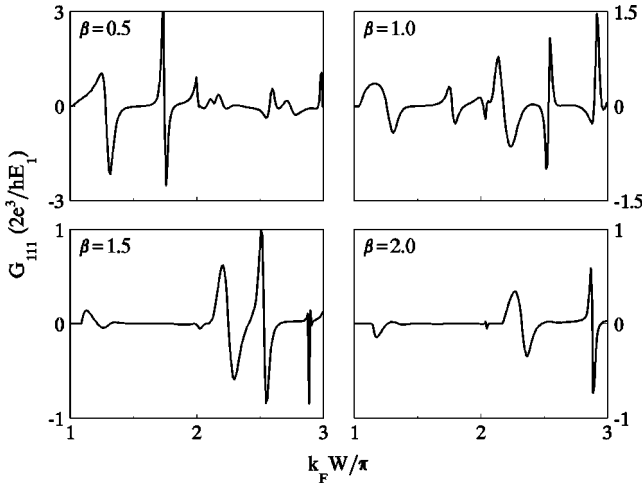


FIG. 6. The leading order nonlinear terms G_{111} as a function of the normalized electron momentum $k_F W/\pi$ for several values of the strength of the magnetic field. Here $E_1 = (\pi/W)^2 \hbar^2 / (2m)$.

which is geometrically symmetrical along the x direction, a more interesting result we found numerically is $\eta_{\alpha\beta}(x,y) = \eta_{\alpha\beta}(-x,y)$. This relation can actually be derived for any symmetric system along the propagation direction, because one can show that the diagonal elements of the retarded Green's function is also symmetric in x . On the other hand the sensitivity is related to the real part of the diagonal elements of the retarded Green's function.¹⁴

In Fig. 6 we plot the nonlinear coefficient G_{111} for several magnetic fields. If there were no \mathbf{B} , $G_{\alpha\beta\gamma}$ must vanish for a symmetric system along the propagation direction, such as for our conductor. This is because $G_{\alpha\beta\gamma}$ is the coefficient of the term quadratic in voltage, thus must be zero for any symmetric system since the current I cannot change when bias $V \rightarrow -V$. However, a magnetic field breaks this symmetry leading to a nonzero $G_{\alpha\beta\gamma}$. The energy dependence of G_{111} is completely different from G_{11} although both have a resonance behavior at small \mathbf{B} . For large \mathbf{B} , while G_{11} is quantized in a steplike fashion, G_{111} still maintains a resonance profile with less resonance peaks and valleys. This is similar to the behavior of the emittance, since both quantities are determined by the behavior of LPDOS. Most interestingly, G_{111} vanishes for most of the energies in a strong magnetic field. This behavior can be partly explained by the fact¹⁴ that the part of G_{111} which corresponds to the external response, is only determined by the energy derivative of the transmission coefficient dT/dE .

The plot of magnetic field dependence of G_{111} enables us to get a clear picture concerning nonlinear magnetotransport. Figure 7 summarizes this result for the present conductor. G_{111} vanishes for $\mathbf{B}=0$ and is negative for a large range of \mathbf{B} . It reaches a negative maximum at a particular field strength. For the system parameters used, this particular strength $\beta \approx 0.6$ leads to a magnetic length $l_B \approx 1.7$. Thus our result suggests that $|G_{111}|$ reaches its maximum value when the magnetic length is compatible to the size of the scattering region. Then, due to the negative value of G_{111} , one may obtain appreciable nonlinear current-voltage characteristics.¹⁶ This outcome is very interesting as it suggests the possibility of using a magnetic field to obtain nega-

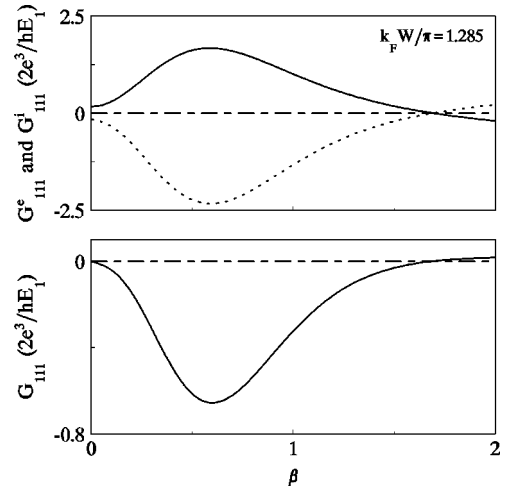


FIG. 7. The leading order nonlinear terms G_{111} as a function of the strength of the magnetic field β at $k_F W/\pi = 1.285$, solid lines for G_{111}^e and dotted lines for G_{111}^i . Here $E_1 = (\pi/W)^2 \hbar^2 / (2m)$.

tive differential resistance. Clearly, for such a situation to occur, higher order nonlinear coefficients may have to be studied as well.

IV. DISCUSSION AND SUMMARY

The scattering matrix theory, when applied to investigate ac as well as nonlinear dc magnetotransport coefficients of coherent quantum conductors, needs to calculate the functional derivatives of the scattering matrix with respect to the scattering potential landscape. This is a difficult problem. In this work we presented a numerical scheme which very effectively solved this problem thus the theoretical formalism can be applied for realistic predictions for complicated 2D or even 3D conductors in the presence of the magnetic field.

The one point that warrants some further discussion is the applicability of this technique when the magnetic field is very high. In that case, as can be expected, any numerical method may have difficulties. The key point of the present method is to match wave functions and their derivatives at an interface with discontinuous confining potential. Under a very high magnetic field, to a large extent the transverse states located on the two sides of an interface would be spatially separated, resulting in a nearly singular behavior in the coupling matrix between the two slices. Under such a situation numerical difficulties occur in this method, leading to a violation of the unitary condition by the numerically obtained scattering matrix. For the T-shaped structure considered in this paper, which represents a typical 2D mesoscopic conductor, the numerical method is stable when field parameter $\beta < 4.0$, and this corresponds to $B < 3.1$ T for $W = 2000$ Å. This is, however, a reasonable field range where most experimental studies are carried out.

The magnetoconductance coefficients under the ac and nonlinear conditions show important dependence on the field strength. Largely speaking the transport features have two main behaviors, one being the usual wave propagation and the other controlled by the edge states. For small field

strength both emittance and the second order nonlinear dc conductance follow the general behavior of the linear dc conductance. In our case this is dominated by the resonance reflections. On the other hand, when edge channels are well formed, ac and nonlinear coefficients change behavior and are strongly determined by the edge picture. A particularly interesting outcome is the purely inductive dynamic response in the ac case and the possibility of obtaining negative differential resistance by controlling the nonlinear coefficient using a magnetic field. Our results also suggest that one may

be able to probe the physics of edge states directly using ac techniques. As demonstrated before,¹² this is a realistic expectation indeed.

ACKNOWLEDGMENTS

We gratefully acknowledge support by a RGC grant from the SAR Government of Hong Kong under Grant No. HKU 7112/97P, a CRCG grant from the University of Hong Kong, the NSERC of Canada and FCAR of Québec. We thank the Computer Center of the University of Hong Kong for computational facilities.

*Present address: Department of Solid State Physics, University of Lund, Box 118, S-22100 Lund, Sweden.

¹For a review, see M. Büttiker, in *Semiconductors and Semimetals*, edited by M. Reed (Academic, New York, 1992), Vol. 35, p. 191.

²P. A. Lee, A. D. Stone, and H. Fukuyama, *Phys. Rev. B* **35**, 1039 (1987); P. A. Lee and A. D. Stone, *Phys. Rev. Lett.* **55**, 1622 (1985); B. L. Al'tshuler, *Pis'ma Zh. Éksp. Teor. Fiz.* **51**, 530 (1985) [*JETP Lett.* **41**, 648 (1985)].

³M. Büttiker, *J. Phys.: Condens. Matter* **5**, 9361 (1993); T. Christen and M. Büttiker, *Phys. Rev. Lett.* **77**, 143 (1996); M. Büttiker and T. Christen, in *Quantum Transport in Semiconductor Submicron Structures*, edited by B. Kramer (Kluwer, Dordrecht, 1996).

⁴T. Christen and M. Büttiker, *Phys. Rev. B* **53**, 2064 (1996).

⁵Y. Meir, N. S. Wingreen, and P. A. Lee, *Phys. Rev. Lett.* **70**, 2601 (1993).

⁶T. K. Ng, *Phys. Rev. Lett.* **70**, 3635 (1993).

⁷N. S. Wingreen, A. P. Jauho, and Y. Meir, *Phys. Rev. B* **48**, 8487 (1993); A. P. Jauho, N. S. Wingreen, and Y. Meir, *ibid.* **50**, 5528 (1994).

⁸C. Bruder and H. Schoeller, *Phys. Rev. Lett.* **72**, 1076 (1994).

⁹M. P. Anantram and S. Datta, *Phys. Rev. B* **51**, 7632 (1995).

¹⁰J. König, H. Schoeller, and G. Schön, *Phys. Rev. Lett.* **76**, 1715 (1996).

¹¹Z. S. Ma, J. Wang, and H. Guo, *Phys. Rev. B* **57**, 9108 (1998); J. Wang, H. Guo, J. L. Mozos, C. C. Wan, G. Taraschi, and Q. R.

Zheng, *Phys. Rev. Lett.* **80**, 4277 (1998); Z. S. Ma, J. Wang, and H. Guo, cond-mat/9712060 (unpublished).

¹²W. Chen, T. P. Smith, M. Büttiker, and M. Shayegan, *Phys. Rev. Lett.* **73**, 146 (1994).

¹³M. Büttiker, H. Thomas, and A. Prêtre, *Z. Phys. B* **94**, 133 (1994).

¹⁴V. Gasparian, T. Christen, and M. Büttiker, *Phys. Rev. A* **54**, 4022 (1996).

¹⁵J. Wang and H. Guo, *Phys. Rev. B* **54**, R11 090 (1996); J. Wang, Q. R. Zheng, and H. Guo, *ibid.* **55**, 9770 (1997).

¹⁶J. Wang, Q. R. Zheng, and H. Guo, *Phys. Rev. B* **55**, 9763 (1997).

¹⁷T. Christen and M. Büttiker, *Europhys. Lett.* **35**, 523 (1996).

¹⁸W. D. Sheng, J. Wang, and H. Guo, *J. Phys. C* **10**, 5335 (1998).

¹⁹T. Christen and M. Büttiker, *Phys. Rev. B* **55**, R1946 (1997).

²⁰F. Sols, M. Macucci, U. Ravaioli, and K. Hess, *Appl. Phys. Lett.* **54**, 350 (1989).

²¹R. L. Schult, D. G. Ravenhall, and H. W. Wyld, *Phys. Rev. B* **39**, 5476 (1989).

²²Y. J. Wang, J. Wang, and H. Guo, *Phys. Rev. B* **49**, 1928 (1994); M. J. McLennan, Y. Lee, and S. Datta, *ibid.* **43**, 13 846 (1991); M. Leng and C. S. Lent, *J. Appl. Phys.* **76**, 2240 (1994).

²³W. D. Sheng, *J. Phys.: Condens. Matter* **9**, 8369 (1997).

²⁴H. Tamura and T. Ando, *Phys. Rev. B* **44**, 1792 (1991).

²⁵H. U. Baranger, D. P. DiVincenzo, R. A. Jalabert, and A. D. Stone, *Phys. Rev. B* **44**, 10 637 (1991).

²⁶Q. R. Zheng, J. Wang, and H. Guo, *Phys. Rev. B* **56**, 12 462 (1997).

²⁷M. K. Yip, J. Wang, and H. Guo, *Z. Phys. B* **104**, 463 (1997).